catalysts

MDPI

Article

Aqueous-Phase Catalytic Chemical Reduction of *p*-Nitrophenol Employing Soluble Gold Nanoparticles with Different Shapes

Francyelle Moura de Oliveira, Lucas Rafael Bezerra de Araújo Nascimento, Claudia Manuela Santos Calado, Mario Roberto Meneghetti * and Monique Gabriella Angelo da Silva *

Grupo de Catálise e Reatividade Química, Instituto de Química e Biotecnologia, Universidade Federal de Alagoas, Av. Lourival de Melo Mota s/n, Cidade Universitária, 57072-900 Maceió-AL, Brazil; fran.moura@hotmail.com.br (F.M.d.O.); lucasr.araujo2@gmail.com (L.R.B.d.A.N.); c.calado@live.com (C.M.S.C.)

* Correspondence: mrm@qui.ufal.br (M.R.M.); monique.silva@qui.ufal.br (M.G.A.d.S.); Tel.: +55-82-3214-1744 (M.R.M.); +55-82-3214-1373 (M.G.A.d.S.)

Academic Editors: Alain Roucoux, Audrey Denicourt and Keith Hohn
Received: 3 November 2016; Accepted: 14 December 2016; Published: 21 December 2016

Abstract: Gold nanoparticles with different shapes were prepared and used as catalysts in the reduction of *p*-nitrophenol (PNP) in the aqueous phase and in the presence of sodium borohydride ($NaBH_4$). Parameters such as the reaction temperature, substrate/$NaBH_4$ molar ratio, and substrate/gold molar ratio were tested and evaluated. In this paper, we compare the catalytic reactivities of gold nanorods (AuNRs) and gold nanospheres (AuNSs), both synthesized by the seed-mediated method in the presence of cetyltrimethyl ammonium bromide (CTAB). Physical-chemical parameters such as the apparent rate constant (k_{app}) and activation energy (E_a) of the reactions were obtained for both systems. We observed that the catalytic system based on AuNRs is the most active. These colloidal dispersions were investigated and fully characterized by ultraviolet-visible absorption spectroscopy (UV–Vis) and transmission electron microscopy (TEM).

Keywords: soluble gold nanoparticles; catalytic chemical reduction; anisotropic nanoparticles; reduction of nitro compounds

1. Introduction

The study and development of new soluble nanocatalysts in water has attracted the attention of several research groups in recent years. Due to their large surface/volume ratio, nanoparticulated catalytic materials can be considered as better catalysts than their bulky form counterparts [1,2]. In recent years, economic and ecological priorities have pressed the scientific community to develop highly active catalytic systems in water for different reactions [3]. It is well known that gold nanoparticles (AuNPs) have received widespread attention due to their interesting physical and chemical properties, particularly in relation to their catalytic activity [4]. In its bulky forms, metallic gold presents low reactivity and has been overlooked for many years as a potential catalyst. However, it was more recently verified that gold nanoparticles are quite active catalysts for many reactions, such as chemical reductions and oxidations [5]. In fact, hydrogenation reactions are the most common reactions that have been conducted using colloidal or supported transition metal nanoparticles. Although gold-based colloids have been widely employed to prepare supported gold catalysts, only a few reports are available in which a liquid colloidal dispersion of AuNPs was employed as the catalytic system [6]. In this context, the synthesis of soluble AuNPs in a high yield with high selectivity in terms of size and shape and the study of their potential applications in catalysis remains the subject of many scientific studies.

It is important to remember that gold has a limited ability to chemisorb hydrogen [7,8] compared to the platinum group metals, and thus, it is a less active catalyst for reactions involving the dissociation of hydrogen [9,10]. Indeed, there are only few works in which molecular hydrogen is employed in the reduction of the chemical species using gold as the catalyst [11]. On the other hand, reduction reactions using $NaBH_4$ catalyzed by supported AuNPs are frequently found in the literature [12]. For example, AuNPs supported on MgO [13], TiO_2 [14], Fe_3O_4 [15], SiO_2 [16], and Fe_2O_3 [17] are used as catalysts in the reduction reactions of nitro compounds, such as *p*-nitrophenol, *p*-nitrotoluene, and their derivatives.

Beyond the homogeneous and heterogeneous classification of catalysts, the morphology [18,19] and size [20–22] of the catalytic particles are crucial factors for nanocatalysis. Indeed, changes in the size and shape of nanoparticles are commonly used to explain the catalytic performance of a specific catalytic material. Although some works revealed that the reactivity and selectivity of reduction in the presence of $NaBH_4$ and catalyzed by AuNPs are dependent on the size and shape of the nanoparticle employed [23,24], with this work we added new aspects that can shed more light on the influence that the size and shape of nanocatalysts has on the performance of a specific catalytic transformation.

Here, we have carried out a series of experiments in order to compare the catalytic reactivities of two AuNPs with different morphologies—gold nanorods (AuNRs) and gold nanospheres (AuNSs)—in the reduction of *p*-nitrophenol (PNP) in the aqueous phase in the presence of sodium borohydride ($NaBH_4$). From those experiments, physical-chemical parameters such as the apparent rate constant (k_{app}) and activation energy (E_a) of the reactions were obtained for both systems.

2. Results and Discussion

The syntheses of the colloidal AuNPs (spheres and rods) were carried out using the same method (seed-mediated) in the presence of cetyltrimethyl ammonium bromide (CTAB). This is an important issue, since the particle-coating molecules display an important role related to the access of the substrates to the catalytic surface. Both colloids were characterized by UV–Vis spectroscopy, and their particles were analyzed by TEM (Figure 1). The absorption spectra of both colloids are typical of systems containing rods and spheres; i.e., two bands with maximum absorptions at 515 and 702 nm, and one band with maximum absorption at 530 nm, respectively. The TEM images confirmed the following trend: AuNSs of approximately 20 nm and AuNRs with dimensions of approximately 40 nm × 12 nm (aspect ratio 3.3) were obtained.

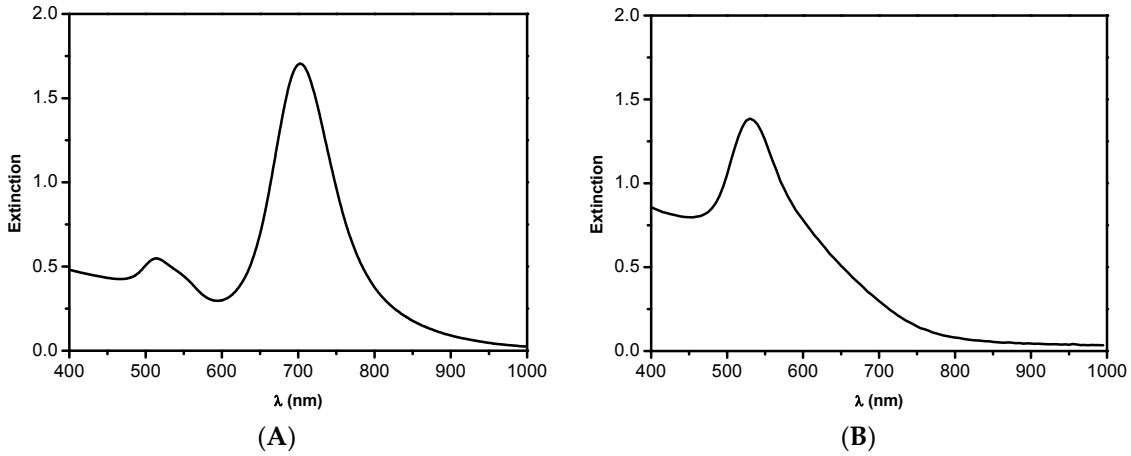

Figure 1. *Cont.*

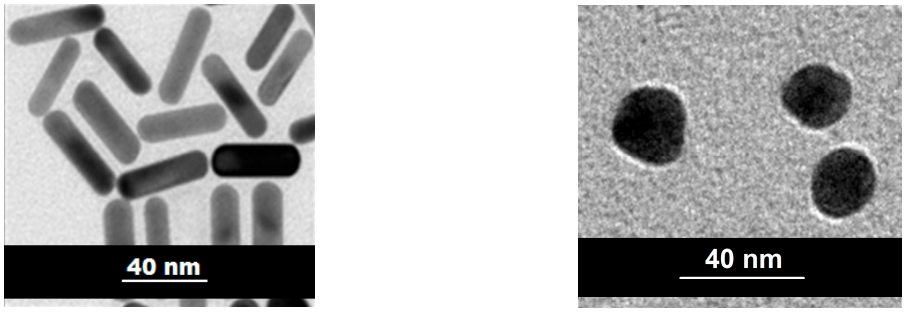

(**C**) (**D**)

Figure 1. Absorption spectra of the colloids containing (**A**) gold nanorods (AuNRs); and (**B**) gold nanospheres (AuNSs). Transmission electron microscopy (TEM) images of the respective nanoparticles (NPs) with dimensions of (**C**) 40 nm × 12 nm for AuNRs; and (**D**) 20 nm for AuNSs, with both having cetyltrimethyl ammonium bromide (CTAB) as the coating species.

2.1. The Catalytic Activity

In this study, *p*-nitrophenol (PNP) was converted into *p*-aminophenol (PAP) in the presence of $NaBH_4$ using AuNSs or AuNRs as nanocatalysts for this chemical transformation. The chemical reduction of PNP was easily followed by UV–Vis spectroscopy. The addition of a specific amount of the gold colloidal solution (catalyst) into the aqueous solution of PNP and $NaBH_4$ starts the reaction, and a sequence of UV–Vis spectra were taken, allowing the kinetics of the conversion of the PNP into PAP to be followed. With the addition of the catalyst, the absorption band at 400 nm related to the substrate (PNP) starts to decrease, while a new band is formed at 300 nm due to product (PAP) formation [13]. It is worth mentioning that due to the reaction conditions, the anionic forms of both PNP and PAP are, in fact, the ones measured. In Figure 2, we can observe a typical example of the trend of the absorption bands related to the consumption of PNP and the formation of PAP during the chemical reduction of the nitro functional group. Moreover, in the absence of the catalysts, no reaction was observed at reasonable times [23].

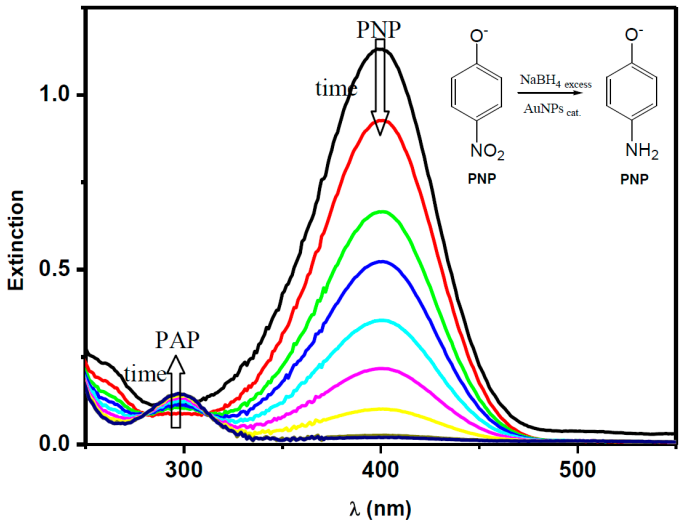

Figure 2. Kinetic studies carried out from a series of UV–Vis absorption spectra obtained during the catalytic chemical reduction of the nitro functional group of *p*-nitrophenol (PNP). PAP: *p*-aminophenol.

For comparison, we have found that both colloidal solutions evaluated are active as catalysts independent of the shape of the AuNPs present in the reduction of PNP in the presence of $NaBH_4$. Here, it is important to mention that only a few reports have discussed the interaction of molecular

hydrogen with gold. Sault and coworkers have shown that no hydrogen chemisorption occurs on the surface [25]. On the other hand, Stobinski and coworkers [26] suggested that some dissociative chemisorption of hydrogen molecules can occur on low coordinated gold atoms (corner and edge sites). Nevertheless, there is a lack of information concerning quantitative data of the adsorption of hydrogen on gold surfaces and supported gold catalysts, but the previously mentioned reasons explain why chemical reductions catalyzed by gold using molecular hydrogen are extremely rare.

The catalytic reduction of PNP in the presence of $NaBH_4$—in which the reduction of the nitro functional group of the molecule is observed—is, in fact, a reaction model usually adopted for the evaluation of potential catalysts. Moreover, the reduction of nitro compounds is a fundamental transformation that occurs in many chemical inputs and intermediates at both laboratory and industrial levels [27]. This catalytic reaction normally occurs with an excess of the hydride source $NaBH_4$, since a considerable part of the activated hydride on the surface of the catalyst is lost as gaseous molecular hydrogen [20,28]. Figure 3 is an illustrative representation of the reaction, with the activation of the hydrides on the surface of the catalyst and their transfer to the nitro group. In fact, according to the literature, in the reduction of nitroarenes using $NaBH_4$ catalyzed by AuNPs, first, a B–H bond cleavage is the rate-determining step to give the [Au]-H species. This species is responsible for the reduction of PNP into the corresponding hydroxylamine [12].

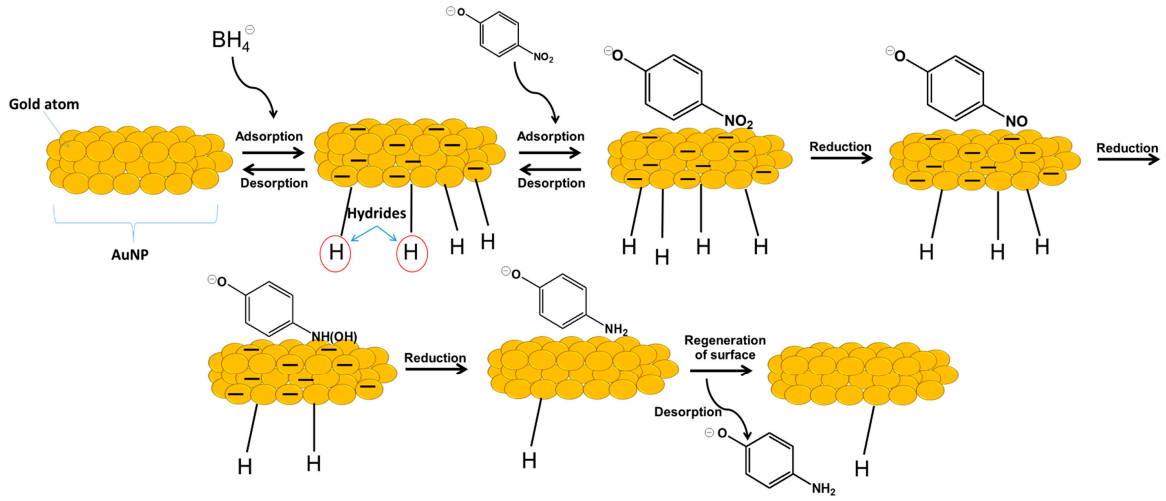

Figure 3. Illustration of the reaction mechanism for the reduction of *p*-nitrophenol catalyzed by gold nanoparticles (AuNPs) in the presence of $NaBH_4$.

In this context, we elaborated a series of experiments to investigate the relationship between the morphology of the nanocatalyst and the catalytic reactivity of the system.

2.2. Influence of the $NaBH_4$ Concentration

This study consisted of evaluating the effect of the modification of the concentration of the reducing agent $NaBH_4$ on the kinetics of the conversion of PNP using both catalytic systems. As we can see in Table 1, the higher the concentration of $NaBH_4$, the faster the reaction is for both systems studied here, confirming that hydride species are involved in the rate-determining step of the reduction reaction of PNP [12].

Table 1. Evaluation of the rate of conversion of PNP using different concentrations of $NaBH_4$ [1].

Entry	[$NaBH_4$] (mol·L^{-1})	$NaBH_4$/PNP Molar Ratio	Conversion Time (s)	
			AuNRs	AuNSs
1	0.10	500	50	266
2	0.05	250	58	340
3	0.025	25	155	555
4	0.0025	12.5	2314	7200

[1] Reaction conditions: 2.0 mL of the PNP solution (0.1 mol·L^{-1}), 1.0 mL of the $NaBH_4$ solution, 0.05 mL of the AuNPs solution (2.0 × 10^{-4} mol·L^{-1}), reaction temperature of 25 °C, and at atmospheric pressure. PNP, *p*-nitrophenol; AuNRs, gold nanorods; AuNSs, gold nanospheres.

In this test, we only analyzed the time necessary to completely convert our substrate. The UV–Vis absorption spectrum as a function of the wavelength allows the conversion of PNP to PAP to be followed. The absorption band at 400 nm indicates the formation of *p*-nitrophenolate, which is formed from the alkaline solution after the addition of $NaBH_4$, and the yellow color of the solution is observed [29]. After the addition of the nanocatalyst, the absorbance band related to the PNP (anionic form) decreases over time, and gradually, a new peak at around 300 nm emerges, corresponding to the formation of PAP (anionic form). Visually, the conversion of PNP is characterized by the modification of the color of the solution from yellow to colorless [13,30].

2.3. The Reaction Temperature

In this study, we carried out a series of reactions of the reduction of PNP in the presence of AuNPs in order to obtain thermodynamic parameters that show how the reaction temperature can affect the kinetics of such a reaction. From Figure 4, it can be seen that the reaction temperature has an important influence. In fact, at higher reaction temperatures, the conversion of PNP is faster. One interesting observation is that when AuNSs are used as the catalyst, the conversion of PNP is significantly slower at 25 °C. This trend shows that the nanocatalyst morphology is indeed an important issue to consider.

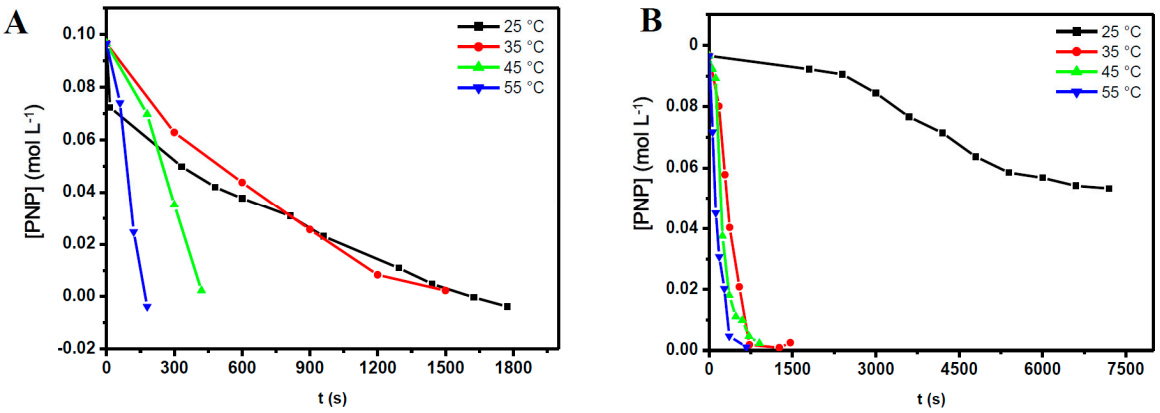

Figure 4. Graphs indicating the modification of the [PNP] during the reduction of PNP versus reaction time at different reaction temperatures using: (**A**) AuNRs; and (**B**) AuNSs as nanocatalysts. Reaction conditions: atmospheric pressure, 2.0 mL of the PNP solution (0.1 mol·L^{-1}), 1.0 mL of the $NaBH_4$ solution, 0.05 mL of the AuNPs solution (2.0 × 10^{-4} mol·L^{-1}), and reaction temperatures of 25, 35, 45, and 55 °C.

To obtain more information about the kinetics of the conversion reaction of PNP, for both catalytic systems, we examined the correlation between ln([PNP]/[PNP]$_0$) and reaction time for all reaction temperatures studied here (see Figures 5 and 6). Supposing, by approximation, that we are under a pseudo-first-order reaction regime for all reactions, linearity must be observed for each set of reaction

conditions. From the slope of the lines, we obtain the apparent rate constant (k_{app}) of the reaction at each set of reaction conditions.

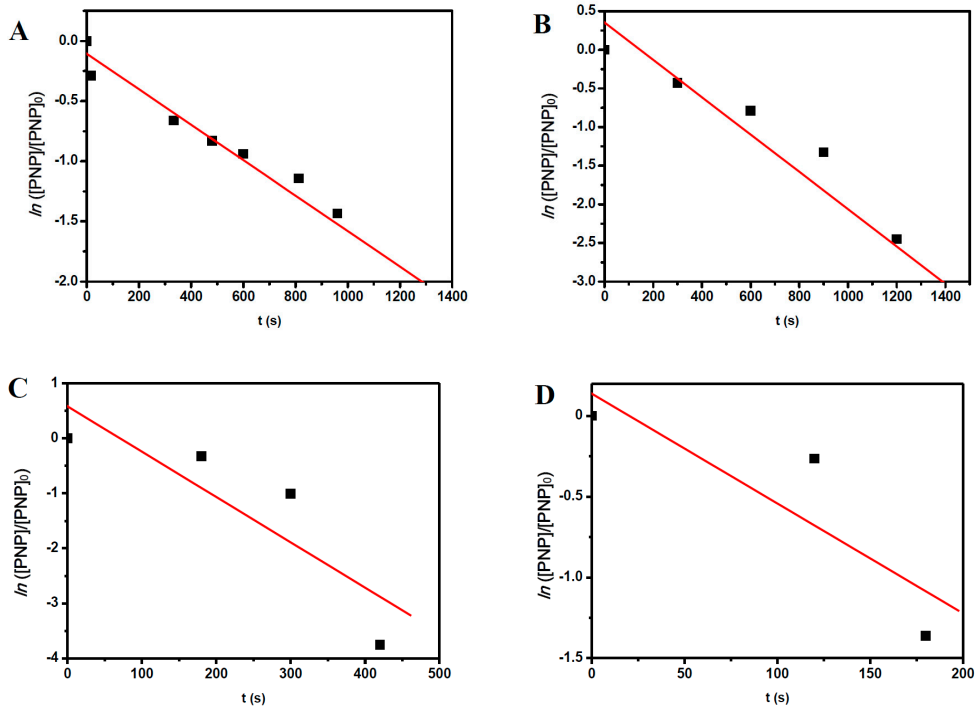

Figure 5. Plots of ln([PNP]/[PNP]$_0$) versus reaction time for the conversion of PNP under different reaction temperatures: (**A**) 25 °C; (**B**) 35 °C; (**C**) 45 °C; and (**D**) 55 °C using AuNRs as the catalyst.

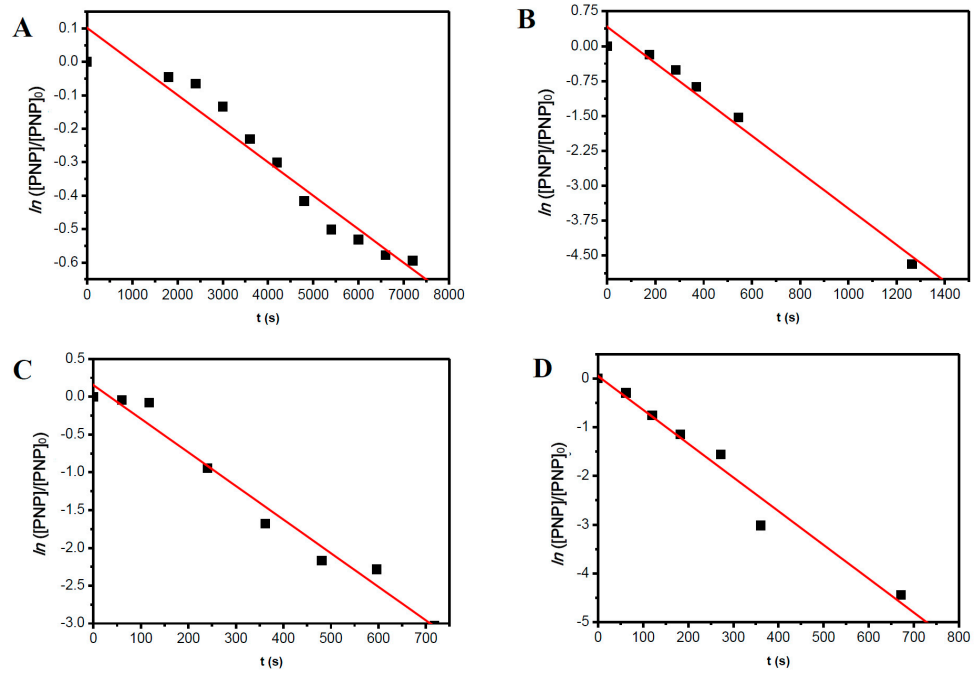

Figure 6. Plots of ln([PNP]/[PNP]$_0$) versus reaction time for the conversion of PNP under different reaction temperatures: (**A**) 25 °C; (**B**) 35 °C; (**C**) 45 °C; and (**D**) 55 °C using AuNSs as the catalyst.

The apparent rate constants obtained for this set of reactions are summarized in Table 2. One can see that at different reaction temperatures, different rate constants are obtained, and as the reaction

temperature increases, the rate constant increases. Nevertheless, it is important to see that the apparent rate constants for the systems using AuNRs as the catalyst are higher. This trend was expected, since the times to reach full conversion of PNP were shorter when AuNRs were used as the catalyst compared to reactions carried out under the same reaction conditions using AuNSs (see Table 1).

Table 2. Apparent rate constants (k_{app}) for the reactions carried out at different temperatures using AuNRs or AuNSs as nanocatalysts.

Temperature (°C)	k_{AuNRs} (s^{-1})	$Error_{AuNRs}$	k_{AuNSs} (s^{-1})	$Error_{AuNSs}$
25	1.0×10^{-3}	$\pm 1.28 \times 10^{-4}$	0.1×10^{-3}	$\pm 8.24 \times 10^{-6}$
35	3.0×10^{-3}	$\pm 4.06 \times 10^{-4}$	3.9×10^{-3}	$\pm 2.74 \times 10^{-4}$
45	14×10^{-3}	± 0.005	4.4×10^{-3}	$\pm 2.9 \times 10^{-4}$
55	18×10^{-3}	-	6.9×10^{-3}	$\pm 5.3 \times 10^{-4}$

Based on the Arrhenius' equation [31], by plotting the graph of the rate constant for each catalytic system versus the corresponding $1/T$ (see Figure 7), one can obtain the activation energy (E_a, apparent) for the reduction reaction of PNP for each catalytic system. From the slopes of the lines, we obtained the following values for E_a: 70 and 105 kJ/mol for the catalytic systems based on AuNRs and AuNSs, respectively.

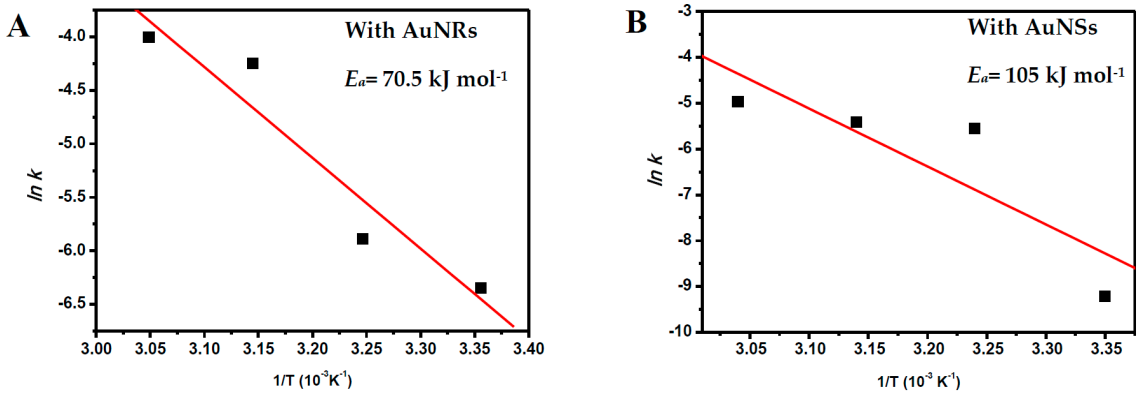

Figure 7. The respective Arrhenius law plots of k_{app} versus 1/T to calculate the activation energy, E_a, from the linear slope for the reduction reaction of PNP catalyzed by (**A**) AuNRs; and (**B**) AuNSs.

It is important to evaluate these results in terms of the particle morphology. As we adopted the seed-mediated method to prepare the AuNPs for both colloidal systems, it is expected that the number of AuNPs in both catalytic systems is the same, as well as the total number of gold atoms. Nevertheless, as they have different morphologies, they can also display different numbers of atoms at their surfaces. Spheres display the lowest relative number of atoms at the surface in comparison to any other geometry. Therefore, under our restrictions of the number of total atoms and number of particles (i.e., both are the same in both catalytic systems), AuNRs should present the higher reactivity. However, it is important to remember that the types of facets, edges, and vertexes of the nanocrystal formed also have an important role for the reactivity of the surface of the nanocatalyst employed [24].

3. Materials and Methods

3.1. General

$HAuCl_4 \cdot 3H_2O$ (99.9%), $NaBH_4$ (99%), (+)-L-ascorbic acid (99%), CTAB, and $AgNO_3$ (99%) were obtained from Sigma-Aldrich (St. Louis, MO, USA) and used as purchased. Distilled water was used to prepare all solutions. UV–Vis/near-IR spectra were recorded on a Shimadzu UV-3600

spectrophotometer (Shimadzu, Kyoto, Japan) using optical glass cells with a length of 1.0 cm. The set-up was configured to fix the baseline of the distilled water absorption band from 200 to 1000 nm. TEM analyses were performed on a FEI Tecnai 20 model electron microscope (FEI, Hillsboro, OR, USA) at an accelerating voltage of 200 kV, and the samples were prepared by the addition of a drop of the gold colloidal solution on a copper grid coated with a porous carbon film.

3.2. Seed-Mediated Synthesis

AuNPs prepared in this study were produced by a seeded-growth method adapted from the protocols developed by Murphy [32] and El-Sayed [33]. The method consists of preparing two solutions: (i) the seed solution; and (ii) the growth solution.

3.2.1. Seed Solution

In a 25 mL flask, 0.1 mL of an aqueous solution of $HAuCl_4 \cdot 3H_2O$ (0.025 mol·L^{-1}, 0.0025 mmol) was added to a 7.4 mL aqueous solution of CTAB (0.0676 mol·L^{-1}, 0.5 mmol). Then, under stirring, 0.6 mL of an ice-cold aqueous solution of $NaBH_4$ (0.01 mol·L^{-1}, 0.006 mmol) was added. The solution color immediately turned to brown. After 2 min, the system was left for at least 2 h without stirring before use.

3.2.2. Growth Solution

In a 25 mL flask, 0.2 mL of an aqueous solution of $HAuCl_4 \cdot 3H_2O$ (0.025 mol·L^{-1}, 0.005 mmol) was added to a 7.3 mL aqueous solution of surfactant (0.0685 mol·L^{-1}, 0.5 mmol). Then, 0.15 mL of an aqueous solution of silver nitrate (4×10^{-3} mol·L^{-1}) was added under stirring, followed by the addition of ascorbic acid (0.070 mL, 0.0788 M). The system turned to colorless, proving the reduction of Au^{3+} to Au^{+}.

3.2.3. Growth Process

A 0.060 mL aliquot of seed particles was added to the freshly prepared growth solution. The solution was kept under stirring for just 10 s and then allowed to stand for 4 h without stirring prior to characterization to ensure system stability.

3.3. Reduction Process in the Presence of $NaBH_4$

All reactions were carried out in a 4 mL glass optical cuvette at atmospheric pressure. Under specific temperatures (25, 35, 45, and 55 °C), the reagents were added in this sequence: 2.0 mL of the PNP aqueous solution (0.1 mol·L^{-1}), 1.0 mL of the aqueous solution of $NaBH_4$ at specific concentrations (0.1, 0.05, 0.025, and 0.0025 mol·L^{-1}), and 0.05 mL of the AuNPs solution (2.0×10^{-4} mol·L^{-1}). The catalytic conversion of PNP was then analyzed by UV–Vis spectroscopy.

4. Conclusions

In this work, we have demonstrated that aqueous colloidal solutions based on soluble AuNRs or AuNSs—both coated with CTAB and produced by seed-mediated method—were catalytically active in the conversion of PNP, producing PAP in the presence of $NaBH_4$. Although the amount of gold used was the same for both catalytic systems, they displayed different catalytic proprieties. The reaction rates for both systems are very sensitive to the reaction temperature, but in all cases, under the same reaction conditions, the k_{app} for the system containing AuNRs as catalyst were higher. This trend was expected, since the time to reach the full conversion of PNP was shorter when AuNRs were used as catalysts. From our results, we could estimate the activation energy of the reduction process of PNP to produce PAP; i.e., 70 kJ/mol and 105 kJ/mol for the catalytic systems based on AuNRs and AuNSs, respectively. It is important to evaluate all results obtained here in light of the particle morphology. As we adopted the seed-mediated method with the same amount of gold to prepare the AuNPs for both colloidal

systems, it is expected that the number of AuNPs in both catalytic systems are the same, as well as the total number of gold atoms. Nevertheless, as they have different morphologies, they can also display different numbers of gold atoms at their surface. Spheres display the lowest relative number of atoms at the surface in comparison to any other geometries. Therefore, under our restrictions of total number of atoms and number of particles, AuNRs should present the higher reactivity. However, it is important to remember that the type of facets, edges, and vertexes of the nanocrystal formed also display important role for the reactivity of the surface of the employed nanocatalyst.

Acknowledgments: The authors are grateful for the financial support financial support from Brazilian research founding agencies, such as Research and Projects Financing (FINEP), National Counsel of Technological and Scientific Development (CNPq), Alagoas Research Support Foundation (FAPEAL), and Instituto Nacional de Ciência e Tecnologia de Catálise em Sistemas Moleculares e Nanoestruturados (INCT-Catálise) is gratefully acknowledged. Mario Roberto Meneghetti thanks CNPq for his research fellowship, and Francyelle Moura de Oliveira, Lucas Rafael Bezerra de Araújo Nascimento, Claudia Manuela Santos Calado thank Coordenação de Aperfeiçoamento de Pessoal de Nível Superior (CAPES), and CNPq for their scholarships.

Author Contributions: All of the authors contributed to the paper. Francyelle Moura de Oliveira, Mario Roberto Meneghetti and Monique Gabriella Angelo da Silva were involved in writing and designing the aim of this manuscript. Francyelle Moura de Oliveira, Lucas Rafael Bezerra de Araújo Nascimento and Claudia Manuela Santos Calado performed the experiments.

Conflicts of Interest: The authors declare no conflict of interest.

References

1. Burda, C.; Chen, X.; Narayanan, R.; El-Sayed, M.A. Chemistry and properties of nanocrystals of different shapes. *Chem. Rev.* **2005**, *105*, 1025–1102. [CrossRef] [PubMed]
2. Narayan, R.; El-Sayed, M.A. Effect of nanocatalysis in colloidal solution on the tetrahedral and cubic nanoparticle shape: Electron-transfer reaction catalyzed by platinum nanoparticles. *J. Phys. Chem. B* **2004**, *108*, 5726–5733. [CrossRef]
3. Bilé, E.G.; Sassine, R.; Denicourt-Nowicki, A.; Launay, F.; Roucoux, A. New ammonium surfactant-stabilizedrhodium(0) colloidal suspensions: Influence of novel counter-anions on physico-chemical andcatalytic properties. *Dalton Trans.* **2011**, *40*, 6524–6531. [CrossRef] [PubMed]
4. Liu, Y.; Xu, L.; Liu, X.; Cao, M. Hybrids of gold nanoparticles with core-shell hyperbranched polymers: Synthesis, characterization, and their high catalytic activity for reduction of 4-nitrophenol. *Catalysts* **2016**, *6*, 3. [CrossRef]
5. Haruta, M. Catalysis of gold nanoparticles deposited on metal oxides. *Cattech* **2002**, *6*, 102–115. [CrossRef]
6. Rossi, M.; Matarrese, R.; Pina, C.D.; Comotti, M. The catalytic activity of "naked" gold particles. *Angew. Chem. Int. Ed.* **2004**, *43*, 5812–5815.
7. Bond, G.C.; Louis, G.C.C.; Thompson, D.T. Reactions involving hydrogen. In *Catalysis by Gold*; World Scientific: Singapore, 2006; Volume 6, pp. 244–268.
8. Hutchings, G.J. Gold catalysis in chemical processing. *Catal. Today* **2002**, *72*, 11–17. [CrossRef]
9. Claus, P.; Brückner, A.; Mohr, C.; Hofmeister, H. Supported gold nanoparticles from quantum dot to mesoscopic size scale: Effect of electronic and structural properties on catalytic hydrogenation of conjugated functional groups. *J. Am. Chem. Soc.* **2000**, *122*, 11430–11439. [CrossRef]
10. Chen, Y.; Qiu, J.; Wang, X.; Xiu, J. Preparation and application of highly dispersed gold nanoparticles supported on silica for catalytic hydrogenation of aromatic nitro compounds. *J. Catal.* **2006**, *242*, 227–230. [CrossRef]
11. Jiang, H.-Y.; Zheng, X.-X. Phosphine-functionalized ionic liquid-stabilized rhodium nanoparticles for selective hydrogenation of aromatic compounds. *Appl. Catal. A* **2015**, *499*, 118–123. [CrossRef]
12. Fountoulaki, S.; Daikopoulou, V.; Gkizis, P.L.; Tamiolakis, I.; Armatas, G.S.; Lykakis, I.N. Mechanistic studies of the reduction of nitroarenes by $NaBH_4$ or hydrosilanes catalyzed by supported gold nanoparticles. *ACS Catal.* **2014**, *4*, 3504–3511. [CrossRef]
13. Layek, K.; Kantam, M.L.; Shirai, M.; Nishio-Hamane, D.; Sasakid, T.; Maheswarana, H. Gold nanoparticles stabilized on nanocrystalline magnesium oxide as an active catalyst for reduction of nitroarenes in aqueous medium at room temperature. *Green. Chem.* **2012**, *14*, 3164–3174. [CrossRef]

14. Tamiolakis, I.; Fountoulaki, S.; Vordos, N.; Lykakisb, I.N.; Armatas, G.S. Mesoporous Au–TiO_2 nanoparticle assemblies as efficient catalysts for the chemoselective reduction of nitro compounds. *J. Mater. Chem. A* **2013**, *1*, 14311–14319. [CrossRef]
15. Leung, K.C.-F.; Xuan, S.; Zhu, X.; Wang, D.; Chak, C.-P.; Lee, S.-F.; Ho, W.K.W.; Chung, B.C.T. Gold and iron oxide hybrid nanocomposite materials. *Chem. Soc. Rev.* **2012**, *41*, 1911–1928. [CrossRef] [PubMed]
16. Liu, H.; Lin, C.; Ma, Z.; Yu, H.; Zhou, S. Gold nanoparticles on mesoporous SiO_2-coated magnetic Fe_3O_4 spheres: A magnetically separatable catalyst with good thermal stability. *Molecules* **2013**, *18*, 14258–14267. [CrossRef] [PubMed]
17. Park, S.; Lee, I.S.; Park, J. A magnetically separable gold catalyst for chemoselective reduction of nitro compounds. *J. Org. Biomol. Chem.* **2013**, *11*, 395–399. [CrossRef] [PubMed]
18. Narayanan, R.; El-Sayed, M.A. Shape-dependent catalytic activity of platinum nanoparticles in colloidal solution. *Nano Lett.* **2004**, *4*, 1343–1348. [CrossRef]
19. Li, J.; Qu, Z.; Qin, Y.; Wang, H. Effect of MnO_2 morphology on the catalytic oxidation of toluene over Ag/MnO_2 catalysts. *Appl. Surf. Sci.* **2016**, *385*, 234–240. [CrossRef]
20. Fenger, R.; Fertitta, E.; Kirmse, H.; Thünemannc, A.F.; Rademann, K. Size dependent catalysis with CTAB-stabilized gold nanoparticles. *Phys. Chem. Chem. Phys.* **2012**, *14*, 9343–9349. [CrossRef] [PubMed]
21. Hinman, J.G.; Stork, A.J.; Varnell, J.A.; Gewirth, A.A.; Murphy, C.J. Seed mediated growth of gold nanorods: Towards nanorod matryoshkas. *Faraday Discuss.* **2016**, *191*, 9–33. [CrossRef] [PubMed]
22. Xiong, W.; Sikdar, D.; Yap, L.W.; Guo, P.; Premaratne, M.; Li, X.; Cheng, W. Matryoshka-caged gold nanorods: Synthesis, plasmonic properties, and catalytic activity. *Nano Res.* **2016**, *9*, 415–423. [CrossRef]
23. Kundu, S.; Lau, S.; Liang, H. Shape-controlled catalysis by cetyltrimethylammonium bromide terminated gold nanospheres, nanorods, and nanoprisms. *J. Phys. Chem. C* **2009**, *113*, 5150–5156. [CrossRef]
24. Soetan, N.; Zarick, H.F.; Banks, C.; Webb, J.A.; Libson, G.; Coppola, A.; Bardhan, R. Morphology-directed catalysis with branched gold nanoantennas. *J. Phys. Chem. C* **2016**, *120*, 10320–10327. [CrossRef]
25. Sault, A.; Madix, R.; Campbell, C. Adsorption of oxygen and hydrogen on Au(110)-(1 × 2). *Surf. Sci.* **1986**, *169*, 347–356. [CrossRef]
26. Stobinski, L.; Zommer, L.; Dus, R. Molecular hydrogen interactions with discontinuous and continuous thin gold films. *Appl. Surf. Sci.* **1999**, *141*, 319–325. [CrossRef]
27. Shokouhimehr, M. Magnetically separable and sustainable nanostructured catalysts for heterogeneous reduction of nitroaromatics. *Catalysts* **2015**, *5*, 534–560. [CrossRef]
28. Goepel, M.; Al-Naji, M.; With, P.; Wagner, G.; Oeckler, O.; Enke, D.; Gläser, R. Hydrogenation of *p*-nitrophenol to *p*-aminophenol as a test reaction for the catalytic activity of supported Pt. *Catal. Chem. Eng. Technol.* **2014**, *37*, 551–554. [CrossRef]
29. Sun, J.; Fu, Y.; He, G.; Sun, X.; Wang, X. Catalytic hydrogenation of nitrophenols and nitrotoluenes over a palladium/graphene nanocomposite. *Catal. Sci. Technol.* **2014**, *4*, 1742–1748. [CrossRef]
30. Johnson, J.A.; Makis, J.J.; Marvin, K.A.; Rodenbusch, S.E.; Stevenson, K.J. Size-dependent hydrogenation of *p*-nitrophenol with Pd nanoparticles synthesized with poly(amido)amine dendrimer templates. *J. Phys. Chem. C* **2013**, *117*, 22644–22651. [CrossRef]
31. Laidler, K.J. *The World of Physical Chemistry*; Oxford University Press: New York, NY, USA, 1993.
32. Murphy, C.J.; Sau, T.K.; Gole, A.M.; Orendorff, C.J.; Gao, J.; Gou, L.; Hunyadi, S.E.; Li, T. Anisotropic metal nanoparticles: Synthesis, assembly, and optical applications. *J. Phys. Chem. B* **2005**, *109*, 13857–13870. [CrossRef] [PubMed]
33. Nikoobakht, B.; El-Sayed, M.A. Preparation and growth mechanism of gold nanorods (NRs) using seed-mediated growth method. *Chem. Mater.* **2003**, *15*, 1957–1962. [CrossRef]